

Supplementary Information

NiCo₂S₄ Sub-Micron Spheres: An Efficient Non-precious Metal Bifunctional Electrocatalyst

Zhongyi Zhang,^{a,b} Xiaogang Wang,^a Guanglei Cui,^{a,*} Aihua Zhang,^d Xinhong Zhou,^c Hongxia Xu,^a Lin Gu,^{d,*}

^a The Qingdao Key Lab of solar energy utilization and energy storage technology, Qingdao Institute of Bioenergy and Bioprocess Technology, Chinese Academy of Sciences, Qingdao, 266101, P. R. China. Fax: 086-0532-80662746; Tel.: 086-0532-80662746; E-mail: cuigl@qibebt.ac.cn

^bCollege of Chemistry and Chemical Engineering, Qingdao University, Qingdao, 266071, P. R. China.

^cQingdao University of Science and Technology, Qingdao, 266042, P. R. China.

^dBeijing Laboratory for Electron Microscopy, Institute of Physics, Chinese Academy of Sciences, Beijing, 100190, P. R. China.E-mail:l.gu@iphy.ac.cn

■ Experimental Details

Synthesis of NiCo₂S₄ Sub-Micron Spheres (SMS)

In typical synthesis, 1 mmol Nickel(II) acetate tetrahydrate ($C_4H_6NiO_4 \cdot 4H_2O$) and 2 mmol Cobalt(II) chloride hexahydrate ($CoCl_2 \cdot 6H_2O$) were mixed with 1 mL 3-mercaptop-1,2-propanediol in a 50 mL three-necked flask, followed by the addition of 20 mL oleyamine (OLA). The mixture was heated to 100 °C and continuously degassed for 30 min and then aerate argon. After that, the solution was heated to 220 °C and kept for 120 min. Subsequently, the solution was cooled to room temperature and then an excess of ethanol was added. The formed precipitate was centrifuged and washed with ethanol for several times, subsequently vacuum-dried at 60 °C. Finally, the purified NiCo₂S₄ sub-micron sphere was obtained.

Physical Characterizations

Scanning electron microscope (SEM) images and energy dispersive spectra (EDS) were acquired using a Hitachi S-4800 field-emission electron microscope. High-resolution transmission electron microscopy (HRTEM) images were acquired using Hitachi H-7650 transmission electron microscopy. X-ray diffraction (XRD) measurements were carried out on a Bruker D8 ADVANCE X-ray diffractometer.

Electrochemical Characterizations

Electrochemical experiments were performed in 0.1 M KOH aqueous using a CHI 440 electrochemical workstation (CHI Instruments Inc.). 5 mg NiCo₂S₄ catalyst was dispersed in a mixture of 950 μL deionized water and 50 μL 5% Nafion solution to prepare a homogeneous ink, and a drop of 10 μL ink was put onto a glass-carbon disk electrode (GCDE, 3 mm diameter) or glassy-carbon rotation disk electrode (RDE, 3 mm diameter) and dried at room temperature, subsequently used as work electrodes. An Ag/AgCl (3 M KCl) electrode and a platinum flake were used as the reference electrode and counter electrode, respectively. For

comparison, commercial Pt/C catalyst (Pt 10 wt.% on carbon, Alfa Aesar) was tested using the same procedure. All potentials are reported relative to the Ag/AgCl (3 M KCl) reference electrode in this study.

The electron transfer number per oxygen molecule involved in the ORR electrocatalyzed by the NiCo₂S₄ SMS is determined by the Koutecky-Levich equation given below.^[1]

$$\frac{1}{j} = \frac{1}{j_k} + \frac{1}{B\omega^{0.5}} \quad (1)$$

Where j_k is the kinetic current and ω is the electrode rotation speed. B could be determined from the slope of K-L plots (Fig. 5b) based on Levich equation as follows:^[2]

$$B = 0.2nF(D_{O_2})^{2/3}\nu^{-1/6}C_{O_2} \quad (2)$$

Where n represents the number of electrons transferred per oxygen molecule, F is the Faraday constant ($F=96485$ C mol⁻¹), D_{O_2} is the diffusion coefficient of O₂ in 0.1 M KOH (1.9×10^{-5} cm² s⁻¹), ν is the kinetic viscosity (0.01 cm² s⁻¹), and C_{O_2} is the bulk concentration of O₂ in 0.1 M KOH (1.2×10^{-6} mol cm⁻³). The constant 0.2 is adopted when the rotation speed is expressed in rpm.^[3]

■ Nitrogen Adsorption-desorption Test

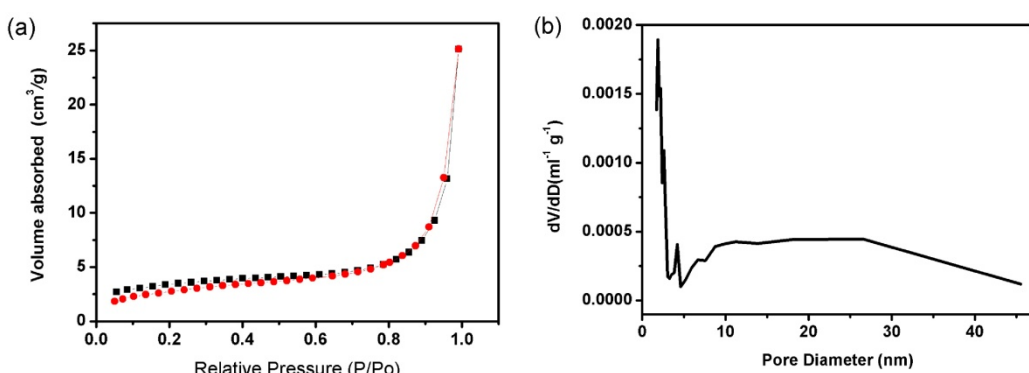


Figure S1 (a) Nitrogen adsorption-desorption isotherms and (b) the pore-size distributions of NiCo_2S_4 SMS.

Figure S1 shows the result of Nitrogen adsorption-desorption test for NiCo_2S_4 SMS. The tested BET surface area of NiCo_2S_4 SMS is $11.5 \text{ m}^2\text{g}^{-1}$. Figure S1b is the pore-size distributions curve, which is shown that the pore diameters of NiCo_2S_4 SMS are primary at 10 nm to 40 nm. Desorption average pore diameter is calculated about 17.3 nm.

■ Other Electrochemical Characterizations

Electro-catalytic activities for ORR and OER

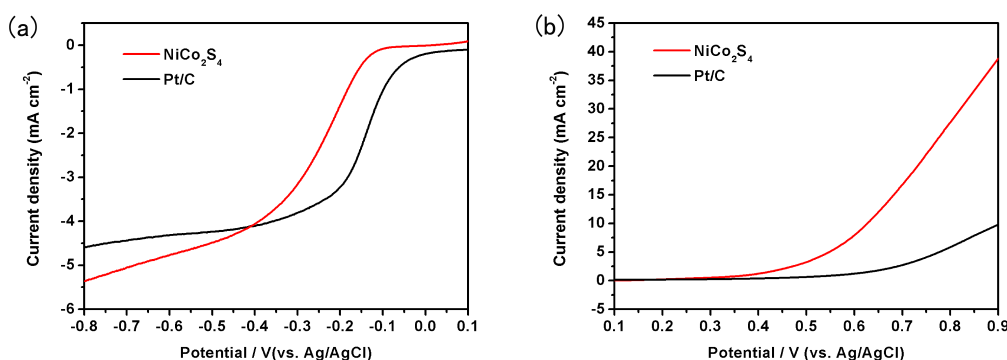


Figure S2 The typical LSV curves for (a) ORR and (b) OER, which were tested on RDE in O₂-saturated 0.1M KOH aqueous solution at 1600rpm with a sweep rate of 10 mVs⁻¹.

Table S1 Benchmarked ORR activities in 0.1 M KOH for Pt and other non-noble alternatives.

Materials	Electrode i (mA cm ⁻²)	Loading (mg cm ⁻²)	Mass i A g ⁻¹	Ref
Pt/C	~4.2	0.7mg	6.0	This work
Co _{0.50} Mo _{0.50} O _y N _z	~4.3	0.7mg	6.1	[4]
NiCo₂S₄	~4.3	0.7mg	6.1	This work
LaNiO ₃	~0.6	0.16mg	3.8	[5]
LaNiO ₃ /C	~1.7	0.16mg	10.6	[5]
LaCu _{0.5} Mn _{0.5} O ₃ /C	~2.5	0.16mg	15.6	[5]

Note: All the ORR activities were tested on RDE at 1600rpm in O₂ saturated 0.1M KOH aqueous solution and corrected at 0.4 V overpotential.

Table S2 Benchmarked OER activities in 0.1 M KOH for IrO₂ and other alternatives.

Materials	Electrode i (mA cm ⁻²)	Loading (mg cm ⁻²)	Mass i A g ⁻¹	Ref
IrO ₂	~18	0.05mg	360	[6,7]
RuO ₂	~15	0.05mg	300	[6,7]
LaNiO ₃	~3.5	0.25mg	14	[7]
La _{0.5} Ca _{0.5} CoO ₃	~3	0.25mg	15	[7]
NiCo₂S₄	~22	0.70mg	31	This work
Ba _{0.5} Sr _{0.5} Co _{0.8} Fe _{0.2} O _x	~20	0.25mg	80	[7]

Note: All the OER activities were tested on RDE at 1600rpm in O₂ saturated 0.1M KOH aqueous solution and corrected at 0.4 V overpotential.

Tafel curves of NiCo₂S₄ SMS and Pt/C for ORR

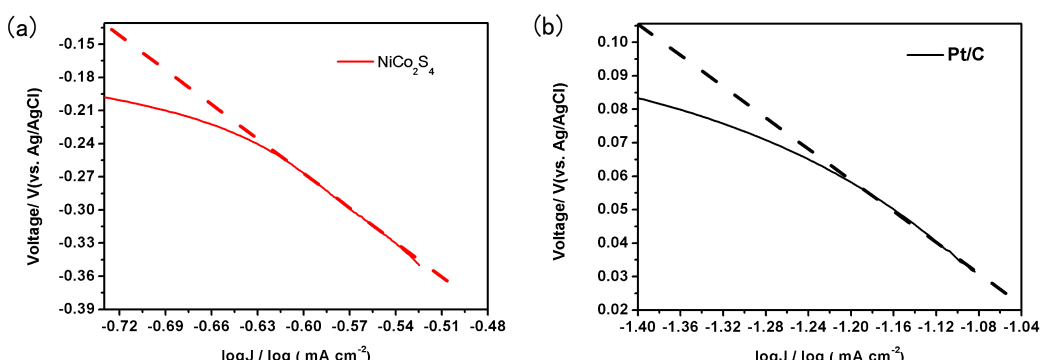


Figure S3 Tafel curves of ORR for (a) NiCo₂S₄ SMS and (b) Pt/C loading on glass carbon electrode in O₂-saturated 0.1M KOH aqueous solution with a sweep rate of 10mVs⁻¹.

The Tafel curves of NiCo₂S₄ SMS and Pt/C catalysts for ORR were shown in Fig. S3. It is calculated that the exchange current density (J_0) for NiCo₂S₄ is around 0.19 mA cm^{-2} . While, for Pt/C catalyst, J_0 is at around 0.04 mA cm^{-2} . The much larger J_0 of NiCo₂S₄ SMS implies a much higher intrinsic electrocatalytic activity for ORR compared with that of Pt/C catalyst.

Chronoamperometric responses for ORR

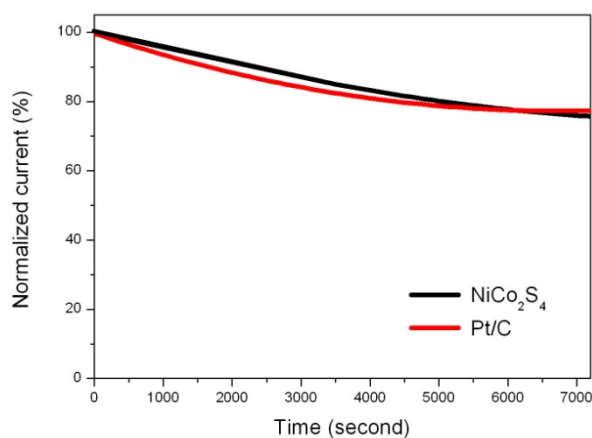


Figure S4 Chronoamperometric responses (percentage of current retained versus operation time) of the NiCo₂S₄ SMS and Pt/C electrocatalysts on glassy carbon electrode in O₂-saturated 0.1 M KOH aqueous solution.

Figure S4 is the chronoamperometric responses of the NiCo₂S₄ SMS and Pt/C electrocatalysts on glassy carbon electrode. As shown in Figure S4, the NiCo₂S₄ electrocatalyst possesses similar stability compared with Pt/C electrocatalyst, which gives a 20% decrease in activity after 7000s of continuous operation.

Tolerance to methanol oxidation in the cathodic reduction of Oxygen

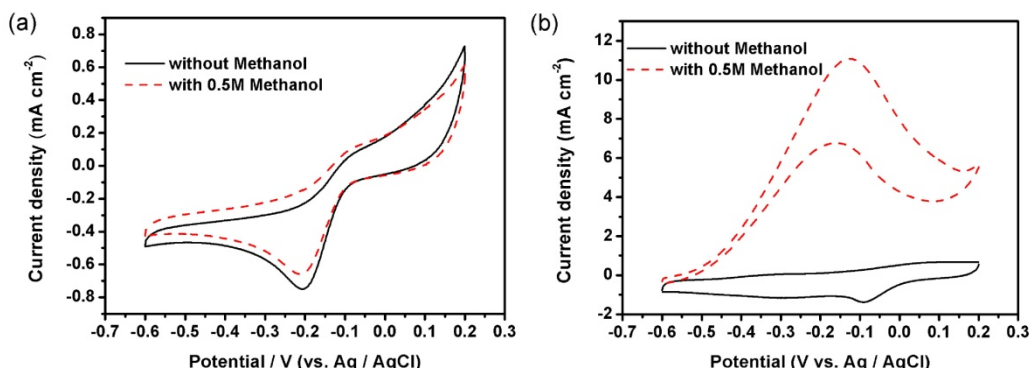


Figure S5 (a) Cyclic voltammetry curves of the NiCo_2S_4 electrocatalyst in O_2 -saturated 0.1 M KOH aqueous solution without methanol (black line) and with 0.5 M methanol (red dash line). (b) Cyclic voltammetry curves of the commercial Pt/C electrocatalyst in O_2 -saturated 0.1 M KOH electrolyte without methanol (black line) and with 0.5 M methanol (red line).

To examine the methanol tolerance of NiCo_2S_4 SMS and Pt/C electrocatalyst, the CV curves in O_2 -saturated 0.1 M KOH aqueous solution with 0.5 M methanol versus the blank test (without methanol) were conducted as shown in Figure S5. In the case of NiCo_2S_4 electrocatalyst, the onset potential and peak current density shows not much change at presence of 0.5 M methanol in solution (Figure S5a). However, for the Pt/C electrocatalyst, the superior strength methanol oxidation peaks appear in the solution contained 0.5 M methanol (Figure S5b). Therefore, NiCo_2S_4 SMS possess high selectivity toward ORR with the advantage of methanol tolerance compared with the commercial Pt/C electrocatalyst.

■ Analysis of Electrocatalytic Mechanism

In order to better gain insight into the electrocatalytic mechanism of NiCo_2S_4 SMS electrocatalyst for both ORR and OER, we resort to detailed analysis of the crystal and electronic structure of NiCo_2S_4 . According to the previous investigation by X-ray and neutron diffraction,^[8] NiCo_2S_4 is indexed to a normal spinel type crystal structure, for which nickel occupies the tetrahedral sites (A-sites) and cobalt occupies the octahedral sites (B-sites). However, the cell edge of the thiocobaltites is about 9.4 Å, which is smaller than the anticipated value for purely ionic structures.^[9] The small sulfur-sulfur distance endows the cobalt-sulfur bands with more covalent character and results in the low-spin state^[2] of the d-electrons for Co(III) : $t_{2g}^6 e_g^0$. Therefore, the σ^* bands associated with Co(III) is empty and any metallic conductivity is due to partially filled bands associated with the A-site of Ni(II) (Fig. S9) in the bulk phase of NiCo_2S_4 , which occupies the center of tetrahedral field and presents high spin state $t_{2g}^4 e_g^4$.

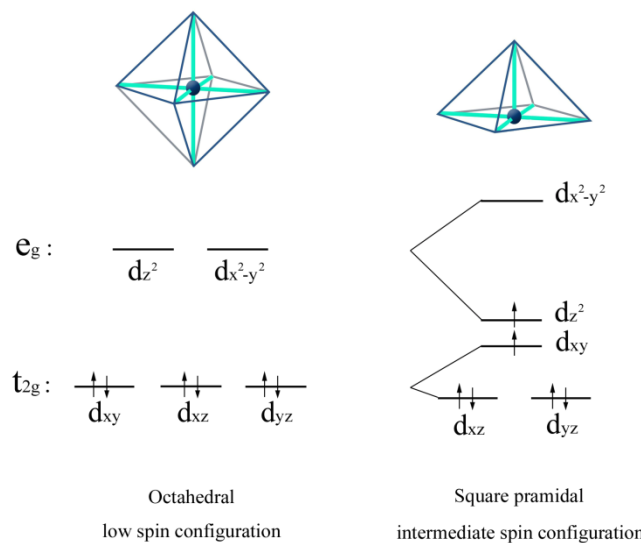


Figure S6 Schematic representation of the energy levels and electronic configurations of d-electrons of Co(III) in bulk phase and on the surface of NiCo_2S_4 crystal particle.

However, on the surface of NiCo_2S_4 crystal particle, the d-electron configuration for Co(III) presents quite different situation from the bulk phase of NiCo_2S_4 crystal particle. The anion

vacancy commonly observed on the surface results in further distortion from octahedral to square pyramidal field (Fig. S6) and exposition of e_g - z^2 orbit (Fig. S7a). Recent reports demonstrated that the surface of CoO_6 octahedral presents the intermediate-spin Co(III): $t_{2g}^5 e_g^1$, instead of the low-spin Co(III): $t_{2g}^6 e_g^0$ in bulk phase.^[10] According to the crystal field theory and the Tsuchida's spectrochemical series,^[11] the splitting energy (Δ) increases with the anion atomic radius reducing. The larger size S^{2-} anion of CoS_6 spinel is much more conducive to this unique spin-state transformation (Fig. S6) compared with the O^{2-} anions of CoO_6 spinel.

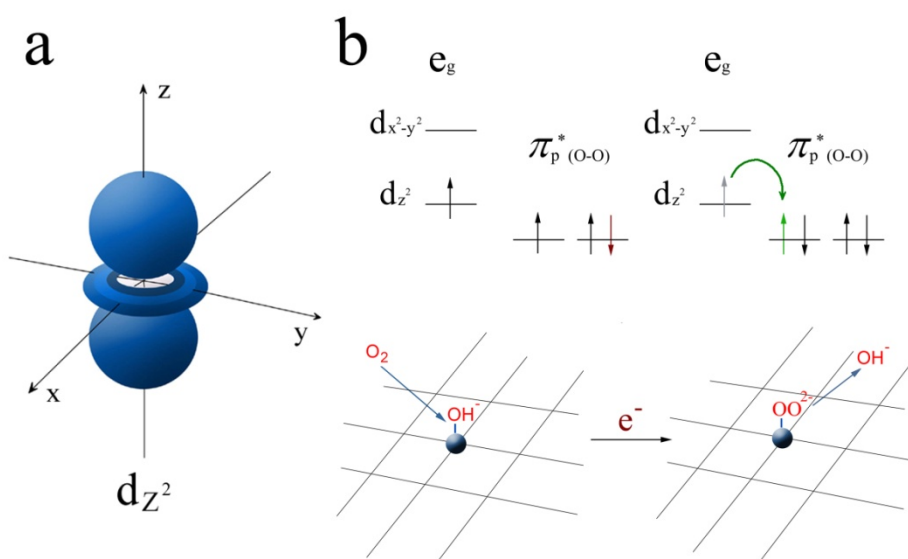


Figure S7 Schematic representation of (a) d_{Z^2} orbit of e_g energy level of Co(III) and (b) the O_2^{2-}/OH^- exchange corresponding to step 1 in ORR reaction.

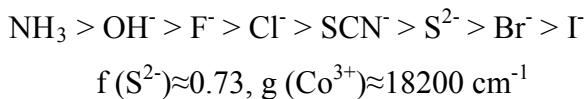
More detailed calculation based on Jorgensen's approximate formula also supports this conclusion as follows:

Theoretical calculations for the d electronic energy levels

According to Jorgensen's approximate formula:

$$10Dq = f(\text{ligand}) \times g(\text{metal})$$

The Tsuchida's spectrochemical series are as follows:



For the sulfur-cobalt atom distance of NiCo_2S_4 is much smaller than that in purely ionic structure,^[9] the corrected 10Dq is as follows:

$$\begin{aligned} 10Dq &= f(\text{S}^{2-}) \times g(\text{Co}^{3+}) \times \left(\frac{R_c}{R_e}\right)^n \\ &= 18200 \times 0.73 \times \left(\frac{9.85}{9.39}\right)^5 \\ &= 16875 \text{ cm}^{-1} \end{aligned}$$

Where $R_c = 9.85\text{\AA}$ ^[12] (calculated cell edge of thiospinel based on ionic S^{2-} without sulfur-sulfur interaction), $R_e = 9.39\text{\AA}$ (the measured cell edge of NiCo_2S_4), $n = 5$ ^[13], for free Co (III) pairing energy = 21000 cm^{-1} . However, for a particular complex, the pairing energy $P = 146700 \text{ cm}^{-1}$. Therefore, in the bulk phase of NiCo_2S_4 for the octahedral CoS_6 :

$$\Delta_o (16875 \text{ cm}^{-1}) > P (146700 \text{ cm}^{-1})$$

Thus, the electronic configuration of d-electrons exhibit low spin-state. While, on the surface of NiCo_2S_4 for the square pyramidal CoS_6 :

$$\begin{aligned} \Delta[dz^2 \sim dxy] &= \{0.86 - (0.86)\} \times Dq \\ &= 1.72Dq \\ &= 2903 \text{ cm}^{-1} \\ \Delta[dx^2-y^2 \sim dyz] &= \{9.41 - (-4.57)\} \times Dq \\ &= 13.98Dq \\ &= 23591 \text{ cm}^{-1} \end{aligned}$$

Therefore,

$$\Delta(z^2-xy) < P < \Delta\{(x^2-y^2)-yz\}$$

Thus, the electronic configuration of d-electrons exhibit intermediate spin-state.

Table S3 Relative energy level of d orbitals represented in D_q

Field structure	d_{z^2}	$d_{x^2-y^2}$	d_{xy}	d_{yz}	d_{zx}
Octahedral	6.00	6.00	-4.00	-4.00	-4.00
Square pyramidal	0.86	9.14	-0.86	-4.57	-4.57

Therefore, the surface Co(III) of CoS₆ spinel is presenting intermediate spin state Co(III):

$t_{2g}^5 e_g^1$, despite the low-spin state Co(III): $t_{2g}^6 e_g^0$ in bulk phase. The single electron in the e_g energy level selectively occupies the e_g - z^2 orbit, which points to the surface sulfur vacancy and dominates the ORR and OER processes (Fig. S8). The importance of single electron for ORR and OER can be explained by the reported proposal of the competition between the O_2^{2-}/OH^- displacement and OH^- regeneration on the surface of metal ions in the alkaline solution.^[14] Figure S10 exhibit the molecular orbital of oxygen, from which it can be seen that the HOMO was constructed by tow degenerated levels of π_{2p}^* . Fig. S7b schematically illustrates the O_2^{2-}/OH^- exchange process corresponding to step1 in ORR reaction (Fig. S8). If the e_g electron filling is more than one, the O_2^{2-}/OH^- exchange does not gain sufficient energy during the displacement process. If the e_g electron filling is less than one, the Co-O²⁻ is not sufficiently destabilized, and subsequently hinders OH^- regeneration, according to the previous literature.^[15] Therefore, the B-site Co(III) as the catalytic center and A-site Ni(II) as the major contributor to electronic conductivity synergistically result in the high performance of NiCo₂S₄ SMS.

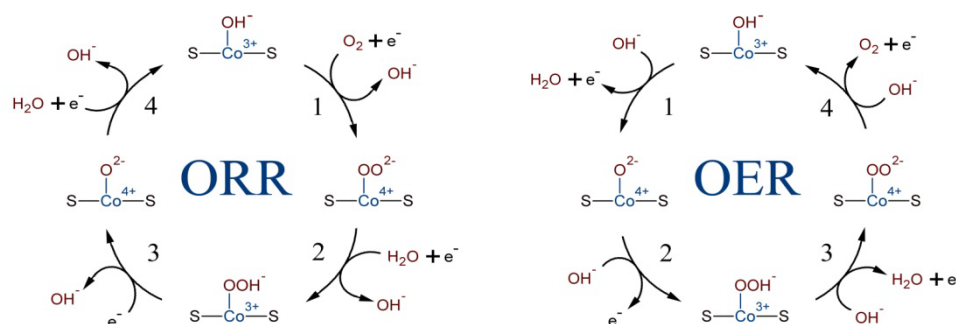


Figure S8 Schematic illustrate of ORR and OER process.

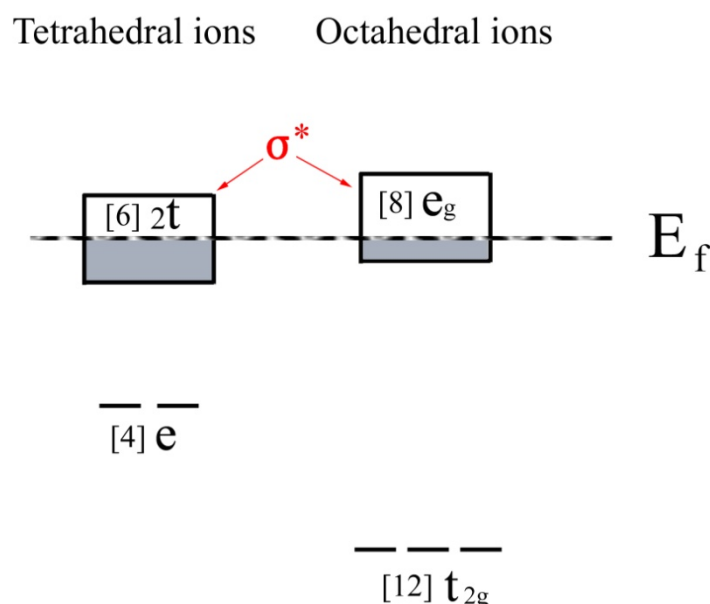


Figure S9 Schematic single-molecule energy diagram for NiCo₂S₄.

In Figure S9, the number in brackets refers to the total degeneracy of a level. These are obtained by multiplying the number of orbital per atom contributing to a level or band by the number of atom per molecule.

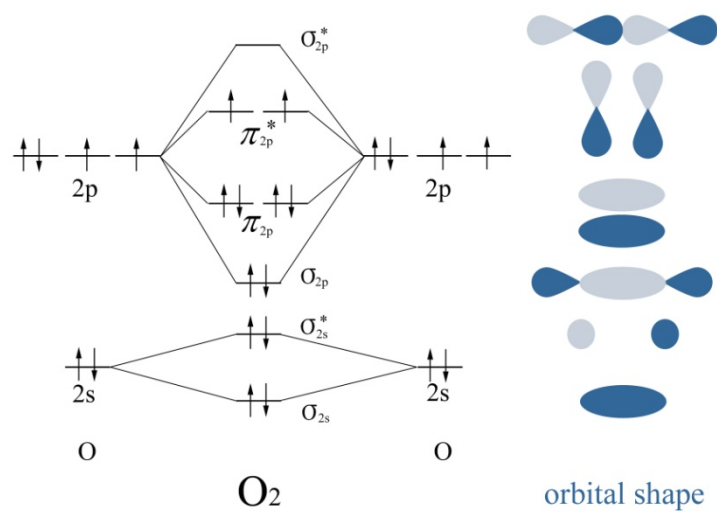


Figure S10 The electronic configuration of the molecular orbital of O_2 .

■ Reference

- 1 D. Yu, Q. Zhang, L. Dai, *J. Am. Chem. Soc.* **2010**, 132, 15127.
- 2 L. T. Qu, Y. Liu, J. B. Baek, L. M. Dai, *ACS Nano.* **2010**, 4, 1321.
- 3 S. Y. Wang, D. S. Yu, L. M. Dai, *J. Am. Chem. Soc.* **2011**, 133, 5182.
- 4 B. F. Cao, G. M. Veith, R. E. Diaz, J. Liu, E. A. Stach, R. R. Adzic, P. G. Khalifah, *Angew. Chem. Int. Ed.* 2013, 52, 10753.
- 5 J. Sunarso, A. A. J. Torriero, W. Zhou, P. C. Howlett, M. Forsyth, *J. Phys. Chem. C* **2012**, 116, 5827.
- 6 Y. M. Lee, J. Suntivich, K. J. May, E. E. Perry, S. H. Yang, *J. Phys. Chem. Lett.* **2012**, 3, 399.
- 7 J. Suntivich, K. J. May, H. A. Gasteiger, J. B. Goodenough, S. H. Yang, *Science* **2011**, 334, 1383.
- 8 O. Knop, K. I. G. Reid, Sutarno, Y. Nakagawa, *Can. J. Chem.* **1968**, 46, 3463.
- 9 A. Wold, K. Dwight, Solid State Chemistry: Synthesis Structure, and Properties of Selected Oxide and Sulfides, P222-228, Chapman and Hall; Softcover reprint of the original 1st ed. **1993**.
- 10 J. Q. Yan, J. S. Zhou, J. B. Goodenough, *Phys. Rev. B* **2004**, 70, 014402.
- 11 T. Ishii, S. Tsuboi, G. Sakane, M. Yamashita, B. K. Breedlove, *Dalton Trans.* **2009**, 680.
- 12 F. K. Lotgering, *Philips Res. Rep.* **1956**, 11, 218.
- 13 P. García-Fernández, J. M. García-Lastra, J. A. Aramburu, M. T. Barriuso, M. Moreno, *Chem Phys Lett.* **2006**, 426, 91.
- 14 J. B. Goodenough, B. L. Cushing, Handbook of Fuel Cells-Fundamentals, Technology and Applications Vol. 2, P520-533, eds Vielstich, W.; Gasteiger, H. A.; Yokokawa, H. (Wiley, 2003).
- 15 Y. Y. Liang, Y. G. Li, H. L. Wang, J. Zhou, J. Wang, T. Regier, H. J. Dai, *Nat. Mater.* **2011**, 10, 780.